

Search for AGN counterparts of unidentified *Fermi*-LAT sources with optical polarimetry

Demonstration of the technique

N. Mandarakas^{1,*}, D. Blinov^{1,2,3}, I. Liodakis⁴, K. Kouroumpatzakis^{1,2}, A. Zezas^{1,2}, G. V. Panopoulou⁵, I. Myserlis⁶,
E. Angelakis⁶, T. Hovatta⁷, S. Kiehlmann⁵, K. Kokolakis^{1,8}, E. Paleologou^{1,2}, A. Pouliasi¹, R. Skalidis^{1,2}, and
V. Pavlidou^{1,2}

¹ Department of Physics and Institute for Theoretical and Computational Physics (ITCP), University of Crete, 71003, Heraklion, Greece

² Foundation for Research and Technology - Hellas, IESL, Voutes, 7110 Heraklion, Greece

³ Astronomical Institute, St. Petersburg State University, Universitetsky pr. 28, Petrodvoretz, 198504 St. Petersburg, Russia

⁴ KIPAC, Stanford University, 452 Lomita Mall, Stanford, CA 94305, USA

⁵ Owens Valley Radio Observatory, California Institute of Technology, Pasadena, CA 91125, USA

⁶ Max-Planck-Institut für Radioastronomie, Auf dem Hügel 69, 53121 Bonn, Germany

⁷ Tuorla Observatory, Department of Physics and Astronomy, University of Turku, Finland

⁸ Geodesy & Geomatics Engineering Lab, Technical University of Crete, GR-73100, Chania, Greece

Received October 18, 2018; accepted January 15, 2019

ABSTRACT

Context. The third *Fermi*-LAT catalog (3FGL) presented the data of the first four years of observations from the *Fermi* Gamma-ray Space Telescope mission. There are 3034 sources, 1010 of which still remain unidentified. Identifying and classifying γ -ray emitters is of high significance with regard to studying high-energy astrophysics.

Aims. We demonstrate that optical polarimetry can be an advantageous and practical tool in the hunt for counterparts of the unidentified γ -ray sources (UGSs).

Methods. Using data from the RoboPol project, we validated that a significant fraction of active galactic nuclei (AGN) associated with 3FGL sources can be identified due to their high optical polarization exceeding that of the field stars. We performed an optical polarimetric survey within 3σ uncertainties of four unidentified 3FGL sources.

Results. We discovered a previously unknown extragalactic object within the positional uncertainty of 3FGL J0221.2+2518. We obtained its spectrum and measured a redshift of $z = 0.0609 \pm 0.0004$. Using these measurements and archival data we demonstrate that this source is a candidate counterpart for 3FGL J0221.2+2518 and most probably is a composite object: a star-forming galaxy accompanied by AGN.

Conclusions. We conclude that polarimetry can be a powerful asset in the search for AGN candidate counterparts for unidentified *Fermi* sources. Future extensive polarimetric surveys at high galactic latitudes (e.g., PASIPHAE) will allow the association of a significant fraction of currently unidentified γ -ray sources.

Key words. Techniques: polarimetric – Galaxies: active – Gamma rays: galaxies

1. Introduction

Since the launch of the *Fermi* spacecraft on 11 June 2008, a vast amount of data has been collected on γ -ray sources. The entire set of point sources detected during the first four years of observations is presented in the 3FGL catalog (Acero et al. 2015). Among the 3034 sources in 3FGL, about one-third (1010) are still unassociated with low-energy counterparts, while AGN account for $\sim 85\%$ of the associations and identifications ($\sim 57\%$ of the entire sample of 3034 sources). In order to classify and associate γ -ray sources, various techniques have been used, as summarized below.

Machine learning. In Doert & Errando (2014), machine learning algorithms were used to find objects with AGN-like properties in the unassociated sources of the 2FGL catalog. Machine training was conducted using 70% of the known AGN in

the catalog, while the remaining 30% were used for testing. Results showed that the algorithm is expected to recognize 80% of the AGN present in the unassociated sample, with a false-association rate of 11%. This technique provided a total of 231 new AGN candidates among the 576 unassociated sources that were studied.

Chiaro et al. (2016) and Salvetti et al. (2017) used the γ -ray variability properties of unassociated sources and neural networks in order to classify these sources. They demonstrated that the percentage of sources of uncertain type in 3FGL can be decreased from 52% to 10% with the use of their method. Similar classification of UGSs can be useful for optimization of surveys dedicated for their identification.

VLBI observations. Kovalev (2009) proposed using very long baseline interferometry (VLBI) for identification of γ -ray sources. The author cross-correlated positions of 205 γ -ray loud sources observed by *Fermi*-LAT with VLBI coordinates of a

* e-mail: nmandarakas@physics.uoc.gr

large sample of extragalactic sources. He was able to confirm the findings of LAT and suggest six new identifications.

Multiwavelength studies. Acero et al. (2013) studied *Fermi*-LAT sources that had also been observed by the Swift satellite with its X-ray telescope (XRT). Swift XRT allowed precise localization at the level of a few arcseconds, with the detected sources being then observed in the radio, IR, or optical. Seven high-latitude sources were investigated, four of which were found to be AGN candidates and one a pulsar candidate. The authors speculated that the two remaining objects may belong to a new category subclass or point to a new type of γ -ray emitter.

Radio spectra. In their search for pulsars in the 3FGL sample, Frail et al. (2016) examined radio spectra of unidentified sources within the 95% confidence error ellipses, using existing catalogs. Compact objects that are bright in MHz frequencies but faint in GHz frequencies were categorized as pulsar candidates.

Radio observations. Barr et al. (2013) conducted radio observations of 289 unassociated sources from the 1FGL catalog using the Effelsberg radio telescope in a search for pulsars. Objects studied were located in the center of their 95% confidence ellipses. Using this method, one millisecond pulsar was discovered.

Schinzel et al. (2017), using the Australia Telescope Compact Array and Very Large Array in the range of 4.0-10.0 GHz, performed a survey of all unidentified *Fermi* sources in the 3FGL catalog, in their search for radio counterparts. They found 2097 candidates, with several fields containing multiple compact radio sources, while others did not contain any above 2 mJy. For several of these targets they performed follow-up observations with VLBI, which provided 142 new AGN associations, alternative associations for 7 objects, improved positions for 144 known associations, as well as 36 extended radio sources. Among the fields studied was 3FGL J0221.2+2518, which is the field of interest of this paper. They propose two possible radio counterparts lying within this field. We discuss the possibility of these associations with the *Fermi* source in Sect. 6.

Figure of merit (FoM). Sowards-Emmerd et al. (2003) used a FoM approach to quantify the probability that an unassociated source is a blazar. To form this FoM, basic characteristics of blazars are taken into account: radio and X-ray properties as well as source position. Based on this approach, the authors evaluated associations of γ -ray and radio sources and presented ~ 20 new identifications.

These methods for the identification of *Fermi* sources make use of various characteristics of γ -ray emitters. Optical polarization is a frequent trait of γ -ray sources that has yet to be exploited in the search for candidate counterparts of yet-unassociated sources.

Blazars are a subclass of AGN with powerful relativistic jets oriented towards our line of sight, which causes strong relativistic boosting of their synchrotron radiation (Blandford & Königl 1979). Due to the synchrotron nature of their optical emission, blazars are often highly polarized in the optical band (Angel & Stockman 1980; Angelakis et al. 2016). Since blazars constitute the majority of γ -ray sources, $\sim 85\%$ of the identified or associated sources and $\sim 57\%$ of the entire 3FGL catalogue (Acero et al. 2015), it is extremely important to be able to distinguish them from other star-like sources in UGS fields. In the next section we investigate the potential of optical polarimetry as a new method for the identification of blazars responsible for UGSs.

The values of the cosmological parameters adopted throughout this work are $H_0 = 67.8 \text{ km s}^{-1} \text{ Mpc}^{-1}$, $\Omega_m = 0.308$, and $\Omega_\Lambda = 1 - \Omega_m$ (Planck Collaboration et al. 2016).

2. Optical polarimetry as a tool for identification of UGSs

2.1. Blazar detection efficiency

While blazars are typically moderately to highly polarized in the optical, they are not the only type of source that can appear polarized in the optical band. We must therefore take into account all processes that produce polarization in the optical, characterize their properties, and finally select the characteristics that isolate blazars from other types of polarized sources. In any given line of sight, light passing through the galactic interstellar medium (ISM) becomes linearly polarized due to dichroic extinction from dust grains that are aligned with the interstellar magnetic field (for a recent review see Andersson et al. 2015). The linear polarization fraction induced by the ISM is typically at a level of a few percent. This can be enough to hinder the identification of a blazar within a typical field. Additionally, the intrinsic fractional polarization of blazars is known to be variable, which can also make them indistinguishable if observed only once at their low-polarization state.

In order to evaluate the efficiency of our method, we developed a Monte Carlo (MC) simulation that allowed us to investigate whether a blazar would be significantly more polarized than foreground stars. To account for the fact that different parts of the sky exhibit different average interstellar polarization and the polarimetric properties in a single region vary between stars in the same region, we relied on the detailed, high-accuracy optopolarimetric mapping of the well-known Polaris Flare cloud using the RoboPol instrument (Panopoulou et al. 2015), and rescaled its polarization properties to different average polarization values that may be applicable at different Galactic latitudes.

First we estimated how much interstellar polarization varies from star to star in an area of the sky that is typical for UGSs position uncertainty. To this end, we found that this area for sources in the 3FGL catalog is 0.0456 deg^2 , which corresponds to a circle with a radius of 0.12 deg. We placed this circle in random positions in the Polaris Flare cloud region and measured the standard deviation of fractional polarization, σ_p , of stars within it, on the condition that there are five or more stars with measured polarization by Panopoulou et al. (2015) within the selected area. We repeated the process until we obtained a set of 5000 σ_p values from which we calculated the standard deviation σ_{σ_p} and the mean M_{σ_p} . Then assuming that at any position on the sky interstellar polarization has the same variance as in the Polaris Flare region, i.e., following the normal distribution $\mathcal{N}(M_{\sigma_p}, \sigma_{\sigma_p})$, we performed the MC simulation as follows:

1. We generated values representing average field polarization in UGSs fields, p_f , in the range $[0\%, 8\%]$, with a step of 0.2%. For each simulated average field polarization we assigned a random σ_f taken from $\mathcal{N}(M_{\sigma_p}, \sigma_{\sigma_p})$ found before.
2. For every value of the average field interstellar polarization (ISP) we drew a random blazar and its intrinsic average polarization p_0 and modulation index m_p from the list of 62 γ -loud blazars presented in Angelakis et al. (2016). This sample is a γ -ray photon-flux limited subsample of 2FGL blazars. It was selected using strict and unbiased criteria making it a representative sample of the parent population of γ -loud blazars.
3. In order to account for their variability properties, for each blazar selected in step 2, we drew a random value for its polarization degree (p_{gen}) from a Beta distribution (Blinov et al.

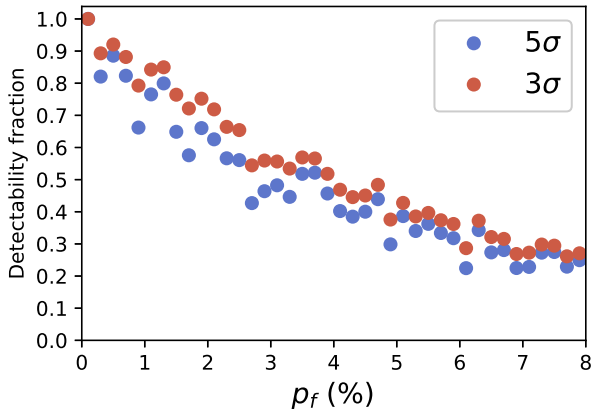


Fig. 1. Percentage of blazars that will stand out 3σ and 5σ from the average polarization of the field p_f .

2016):

$$\alpha(p_0, m_p) = \left(\frac{1 - p_0}{p_0 m_p^2} - 1 \right) p_0, \quad (1)$$

$$\beta(p_0, m_p) = \left(\frac{1 - p_0}{p_0 m_p^2} - 1 \right) (1 - p_0). \quad (2)$$

4. We considered a blazar to be significantly more polarized than the field stars (i.e., detectable) if $p_{gen} > p_f + SL \times \sigma_f$, where the significance level (SL) is the number of standard deviations.

Repeating the simulation 10^3 times for $SL = 3$ and 5 , we found the expected fraction of the fields where the UGS could be detected (in the case where the UGS is associated with a blazar) using optical polarization measurements. The results of the simulation are shown in Fig. 1. It follows from this plot that for high galactic latitudes ($|b| > 10^\circ$), where the average field polarization is expected to be $\leq 1\%$, $\sim 80\%$ of the blazars in UGSs will be 3σ more polarized than the background ISP.

2.2. Expected number of detections

In order to estimate the number of sources among UGSs that can be detected in a polarimetric survey, we performed the following MC simulation. For each UGS we found the reddening $E(B - V)$ from Schlafly & Finkbeiner (2011). Then we estimated the maximum possible ISP value for each field following the relation by Hiltner (1956):

$$P_{\max} \leq 9E(B - V)(\%/mag). \quad (3)$$

After assigning random optical polarization P_r for each source following the procedure describe dabove, we considered an UGS to be suitable for detection when $P_r \geq P_{\max}$. Repeating this simulation 10^4 times we found that if $\sim 85\%$ of unidentified sources are blazars (as it is for identified sources in 3FGL), then 526 ± 9 could be detected using optical polarimetry.

We note that equation 3 significantly overestimates ISP for high extinction regions because high extinction values are reached in the case of multiple foreground dust screens, while it is unlikely that the magnetic field is perfectly aligned within these regions with respect to each other. Therefore, above some level of $E(B - V)$ the increase of ISP halts due to depolarization

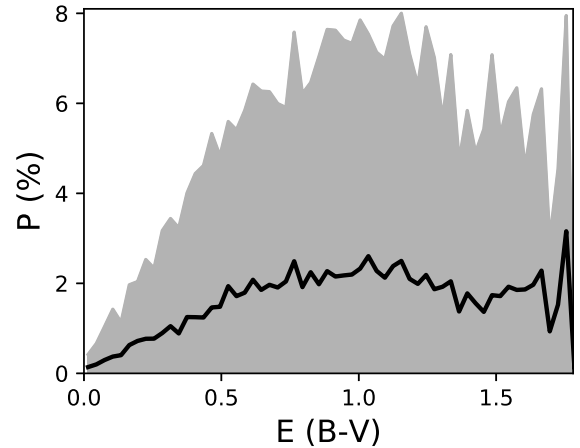


Fig. 2. Dependence of stellar polarization from Heiles (2000) with the corresponding reddening from Schlafly et al. (2014). The black line represents the mean polarization of stars within 0.03 mag bin of $E(B - V)$. The gray area shows 3 standard deviations from the mean.

caused by the diverse magnetic field directions in different polarizing screens. Moreover, the recalibration of extinction maps of Schlafly et al. (1998) provided by Schlafly & Finkbeiner (2011) may be inaccurate outside of the Sloan Digital Sky Survey footprint (Schlafly et al. 2014). These two factors lead us to repeat the estimation of the number of detectable sources using a different approach.

Using 5590 stars with high signal-to-noise ratio measurements ($P/\sigma_P > 3$) from Heiles (2000) and the dust reddening map by Schlafly et al. (2014) we found the dependence of P on $E(B - V)$. For each star with a polarization measurement we found the corresponding reddening value, then we split the entire range of reddening into bins of 0.03 mag and calculated the mean p_{redd} and the standard deviation σ_{redd} of polarization for the stars within each bin. The obtained dependence is shown in Fig. 2. Then for each UGS we found $E(B - V)$ from Schlafly et al. (2014)¹ and assigned a corresponding p_{redd} and σ_{redd} using the dependence in Fig. 2. For UGSs with $E(B - V) > 1.75$, which is outside the range covered by Heiles (2000), stars were assigned $p_{redd} = 100\%$. After that we repeated step 4 from Sect. 2.1 and assigned each source a random polarization P_r following the beta distribution and parameters of real blazars from Angelakis et al. (2016). Then we repeated the last step 10^4 times computing the fraction of sources where $P_r > p_{redd} + 3 \times \sigma_{redd}$. We found that in the case where 85% of currently unidentified 3FGL sources are blazars, we expect to be able to detect 544 ± 10 of them in an optical polarization survey, which is consistent with the previous rougher estimate.

It is worth noting that our simulations take into account only polarization degree while the direction of polarization plane is omitted. A more accurate approach must take into account the vector nature of linear polarization. Observed polarization of a blazar is a vector sum of its intrinsic and the interstellar polarizations. For this reason even blazars with intrinsic polarization values lower than the average interstellar field polarization can be detected if the polarization angles of the two significantly differ. Therefore, the efficiency of the technique may in fact be even higher than the estimate presented above.

¹ In the case when it was outside the footprint of Schlafly et al. (2014), we used $E(B - V)$ from Schlafly & Finkbeiner (2011).

Table 1. Data information and ranking parameters of the four observed sources along with their sequential position in the list sorted by ranking. Flx is measured in 10^{-8} ph cm $^{-2}$ s $^{-1}$ and Pos in deg 2 .

3FGL id	Flx	Var	Pos	Rank.Par.	Position
J1848.6+3232	2.84	193	0.01	551	31
J0419.1+6636	2.2	49	0.008	130	106
J0336.1+7500	1.06	34	0.007	52	219
J0221.2+2518	0.45	38	0.024	7	660

2.3. Survey strategy

Before proceeding to put the method to the test, we established a ranking parameter to quantify the possibility of detecting a blazar in a *Fermi*-LAT region. In other words, we characterized fields by suitability for follow-up observation. We define the ranking parameter as $R = (Var \times Flx \times 10^6)/Pos$. The variables affecting this parameter are the following:

- *Variability (Var)*: Sources from 3FGL are flagged with a *Var* index, which denotes the probability of a source to be variable (Acero et al. 2015). High values of *Var* denote a higher probability that the source is an AGN.
- *γ -ray photon flux (Flx)*: Given our current understanding of the relation between optical and γ -rays, a high photon flux in the range 100 MeV – 100 GeV would suggest a high optical flux density if the source responsible for the γ -ray emission is an AGN (e.g., Cohen et al. 2014; Liodakis et al. 2018).
- *Positional error (Pos)*: The positional error determined as the area of an ellipse encircling the 95% confidence region of *Fermi* sources locations. It is given in deg 2 and is calculated as $\pi \times a \times b$, where *a* and *b* are semi-major and semi-minor axes of the positional error ellipse provided in 3FGL. The larger the positional error, the more difficult it is to study the area.

The ranking parameter ensures that the target field under investigation contains a variable, γ -ray bright source within a relatively small region of the sky.

We observed fields of four UGSs with various ranking parameters. These sources were selected randomly among all visible UGSs at the moment of observations. Their ranking parameters and the sequential positions in the list of 1010 unidentified *Fermi* sources sorted by the rank are presented in Table 1.

3. Observations and data reduction

Polarimetric data of the targets were obtained using the RoboPol² polarimeter attached to the 1.3m. telescope at the Skinakas observatory (35.2120°N, 24.8982°E) located in Crete, Greece. RoboPol contains a combination of two Wollaston prisms and two half-wave plates simultaneously splitting incoming light in four different polarization directions, which are then projected as a four-point image for each source on the CCD. The only moving part is its filter wheel, which is equipped with B, V, R, I Johnson-Cousins filters. The particular design of the RoboPol polarimeter allows the measurement of the Stokes parameters with a single exposure, thereby minimizing systematic and statistical errors. The instrument is optimized for measurements of a source at the center of its 13' \times 13' field of view by a mask in the telescope focal plane. The mask has a cross-shaped aperture in the center and is designed to block unwanted photons from the nearby area of the central source, as well as

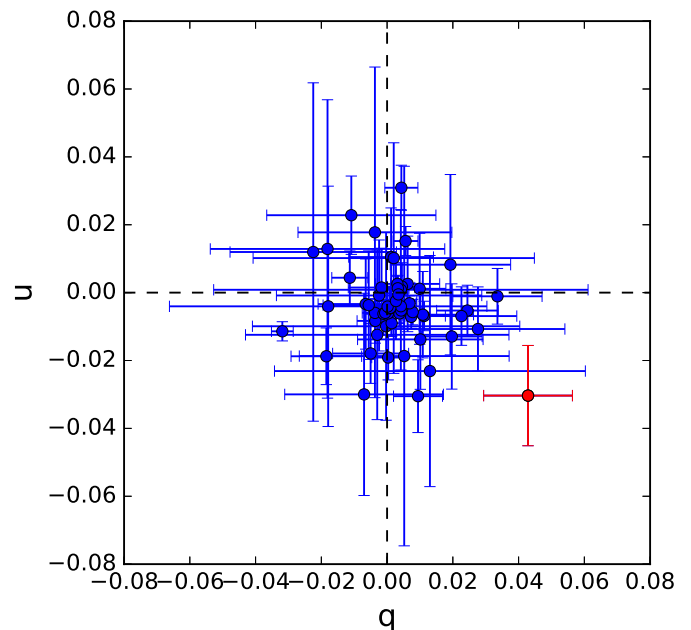


Fig. 3. Distribution of *q* and *u* Stokes parameters of field sources. UGSC is shown by the red symbol.

nearby sources from overlapping with it. The background noise surrounding the spots is reduced by a factor of 4 compared to field sources, allowing more precise and reliable measurements. RoboPol was primarily designed to monitor the optical linear polarization of blazars, with the first observations taking place in June 2013 (Pavlidou et al. 2014).

The operation of the instrument and data reduction is based on an automated pipeline described in detail by King et al. (2014). Although the pipeline processes the entire RoboPol field of view, there are certain issues that need to be taken into account when performing and analyzing field measurements. The issues affecting our measurements are briefly discussed below.

- *Large scale optical aberrations*: Aberrations caused by the optical system are corrected by the instrument model described in King et al. (2014), and improved by Panopoulou et al. (2015). In the latter paper there is also an estimate of the residual uncertainty after the instrumental model correction.

- *Proximity of two sources*: Since RoboPol produces a four-point image for each source, it is common for one or more of these points to overlap with a point from a nearby source. Such sources are excluded from the analysis on condition that a spot exists within $3 \times \text{FWHM}$ of another source's spot.

- *Proximity to the CCD edges*: Sources close to the CCD edges are very likely to suffer from partial photon losses; i.e., one or more of the four spots are not projected on the CCD image. Consequently, sources falling 100 pixels or less from the edges are rejected from the analysis.

- *Aperture optimization*: Stokes parameters $q=Q/I$ and $u=U/I$ are calculated through aperture photometry in each of the four spots of the same source. A number of conditions may affect the PSF of the spots (e.g., weather, seeing, optical system); therefore, it is necessary to employ different photometry parameters for each of the spots. We account for this using an aperture optimization algorithm (Panopoulou et al. 2015).

- *Dust specks*: Telescope and RoboPol optics could be contaminated with dust resulting in specks on the produced CCD

² <http://robopol.org/>

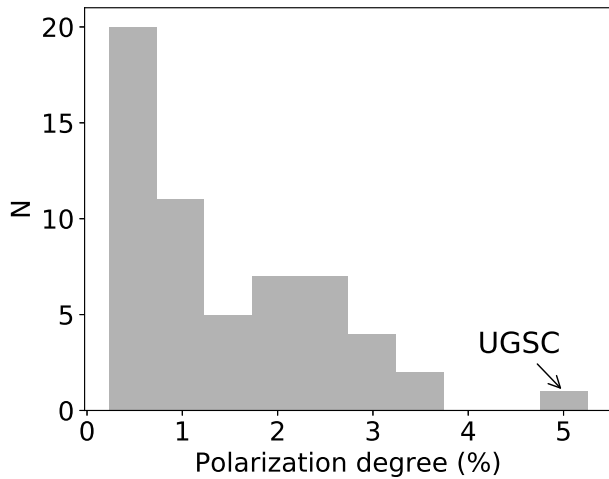


Fig. 4. Distribution of the polarization values for the 57 sources in the 3FGL J0221.2+2518 field.

image. Objects falling on the dust specks are removed from the analysis.

For a more detailed description of errors in field measurements and corresponding solutions, refer to Panopoulou et al. (2015).

We performed measurements of the sources within 3σ positional uncertainties of the four UGSs listed in Table 1 using the RoboPol instrument in August – October 2017. Observations were conducted in the R band. For each field we obtained 3×190 sec exposures at five positions of the telescope, separated by 1.2 arcmin, and having a square shape with one pointing in the center.

4. Results

For the first three UGS fields, despite their high ranking parameters, we do not find any source that has significantly higher optical polarization than the average value for the field. However, in the case of 3FGL J0221.2+2518 we detect an outlier. Here we focus only on this UGS.

Analysis of the field provided us with reliable polarization measurements for 57 sources in the field of interest. Although there are many more objects within 3FGL J0221.2+2518 field, sources fainter than 18th magnitude were not taken into account due to their high measurement uncertainties. In addition, a number of moderately bright sources were excluded from the analysis or could not be resolved due to issues discussed in Sect. 3. After processing the results of the analysis, we observed the objects with the highest polarization in the mask of RoboPol to acquire more accurate measurements.

The values of q and u are represented in Fig. 3 and the corresponding distribution of fractional polarization values is shown in Fig. 4. There is a source with polarization degree $5.2 \pm 1.3\%$ clearly deviating from the median polarization degree across the field ($p_{av} = 0.91 \pm 0.07\%$) that qualifies as a γ -ray emitting candidate. The Unidentified Gamma-ray Source Candidate (UGSC) is located at RA=02h21m33.3s, Dec=+25° 12' 47.2'' (J2000), and its position with respect to the *Fermi* source is presented in Fig. 5. It is listed in SDSS as J022133.31+251247.3 with $r = 17.59$ mag. This source is not presented in any known AGN catalogue. The polarization degree of UGSC (albeit moderate compared to bonafide blazars) indicates synchrotron emission as its origin; however, other mechanisms are possible. For instance,

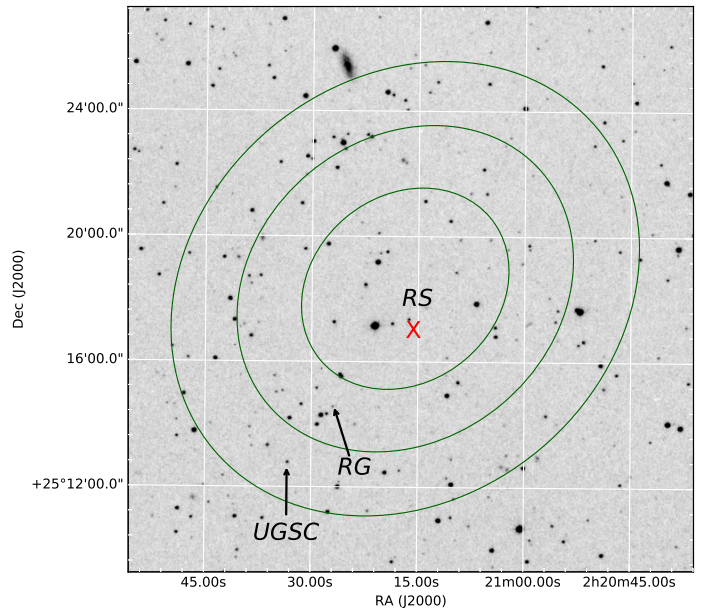


Fig. 5. DSS image of 3FGL J0221.2+2518 field and the position of UGSC and other candidates for the field as discussed in Sect. 6. *RS* and *RG* are the two candidates proposed by Schinzel et al. (2017) and stand for radio source and radio galaxy, respectively. The ellipses represent 1σ , 2σ , and 3σ uncertainties of the γ -ray source position.

the polarization degree up to 4% can be reached due to the scattering in circumstellar discs of Be/X-ray binaries (Halonen et al. 2013) or pre-main sequence stars (Oudmaijer et al. 2001). Therefore, we collected additional archival data and performed supplementary optical spectroscopic observations in order to validate its AGN nature, as presented in the following section.

5. Evidence of AGN nature of the UGSC

5.1. Optical spectrum and redshift

Even though the UGSC is in the SDSS catalogue, it does not have an available spectrum. Therefore, we obtained a spectrum of this source, using the 1.3 m telescope of the Skinakas observatory. The spectrograph is equipped with an ANDOR DZ436 CCD camera with 2048×2048 pixels and a 651 lines/mm grating, giving a nominal dispersion of ~ 1.85 Å/pixel. The total exposure time was 4500 sec divided in three exposures. The spectrum was processed using the standard IRAF (version 2.16.1) CCD reduction, optimal extraction, and calibration. The spectrum is shown in Fig. 6. It is not flux-calibrated since it is not necessary for performing line intensity ratio calculations. Different distortions can be caused in the intensity of the spectrum in different wavelengths. In our case, emission lines are close, thus their relative intensity weakly depends on the wavelength.

We identified H_β 4863Å and [OIII] 5008Å lines, as well as H_α 6565Å, [NII] 6550Å, 6585Å, and [SII] 6718Å, 6733Å lines. Using these lines, we calculated the redshift of the source: $z = 0.0609 \pm 0.0004$. According to the intensity ratios of the emission lines, $\log(\frac{[\text{NII}]_{6585}}{H_\alpha}) = -0.360 \pm 0.005$, $\log(\frac{[\text{SII}]_{6718,6733}}{H_\alpha}) = -0.512 \pm 0.005$, and $\log(\frac{[\text{OIII}]}{H_\beta}) = -0.49 \pm 0.03$, we determined the position of the UGSC on the Baldwin-Phillips-Terlevich (BPT) diagrams, as revised by Kewley et al. (2006). It is shown in Fig. 7. BPT diagrams were originally presented by Baldwin et al. (1981) and are used as diagnostic diagrams to classify galaxies

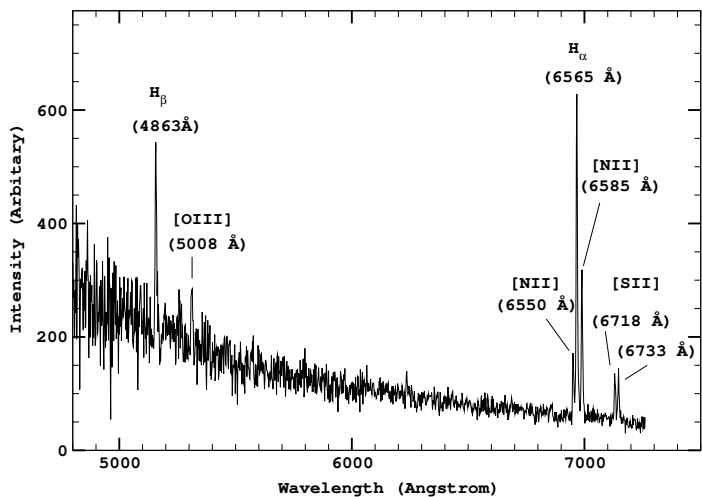


Fig. 6. Optical spectrum of UGSC. Presented are the lines that were identified along with their rest frame wavelength.

based on their emission lines. UGSC lies in the star-forming region of the diagram, right below the Ka03 line. In Sect. 5.4 we show that UGSC is most likely a starburst galaxy with an AGN core.

5.2. X-ray data

In order to collect additional information on UGSC, we proceeded to acquire X-ray data. The field around the source was observed on 9 September 2018 under our ToO request with XRT onboard *Neil Gehrels Swift* observatory (Burrows et al. 2005). The total exposure time was 1900 sec. We used the xselect FTOOL³ (Blackburn 1995) with the cleaned event files produced from the standard pipeline in order to extract an image in the 0.5–8.0 keV band. We do not detect any significant X-ray source at the location of the candidate optical counterpart. Based on the number of counts within an aperture of 0.5'' radius (and an estimate of the background from a nearby source-free region), we calculate a source intensity of $9.89^{+10.2}_{-6.9} \times 10^{-4}$ count/sec (0.5–8.0 keV) at 68% confidence based on the BEHR algorithm (Park et al. 2006). Assuming a $\Gamma = 1.7$ power-law model absorbed by the Galactic line-of-sight column density ($N_H = 6.6 \times 10^{20} \text{ cm}^{-2}$ (Dickey & Lockman 1990)), this count rate corresponds to an observed flux of $3.85^{+3.97}_{-2.69} \times 10^{-14}$ erg/s/cm² and a luminosity of $3.7^{+3.8}_{-2.6} \times 10^{41}$ erg/s (0.5–8.0 keV band). Therefore, we consider $\sim 7.4 \times 10^{41}$ erg/s as the 68% confidence upper limit on its X-ray luminosity.

5.3. Broadband spectral energy distribution

We collected archival broadband photometry available for UGSC including measurements by the WISE, 2MASS, SDSS, Gaia, and GALEX surveys. The combined spectral energy distribution (SED) including the X-ray upper limit from the previous section is shown in Fig. 8. It shows signs of three peaks that are presumably consistent with a presence of three emission components. The mid-infrared peak can be produced by a dusty torus. The peak with a maximum in the optical bands can be caused by the underlying galaxy stars emission. While the possible rise towards hard UV in the GALEX bands could be explained by the accretion disk emission. However, we note that the data from the

surveys are not contemporaneous and may represent the source at different activity states, which in turn can cause a semblant multicomponent SED.

We plot the γ -ray data of 3FGL J0221.2+2518 from 3FGL on the same SED under the assumption that it is associated with UGSC. The overall SED shape and its components are consistent with the SEDs of known γ -ray emitting NLSy1 (Foschini et al. 2012; Paliya et al. 2018). However, the luminosity $L_\gamma = 3.7 \pm 0.9 \times 10^{43}$ erg/s of the UGSC is more than an order of magnitude lower than any other NLSy1. Moreover, near- to mid-infrared colors, $[3.4\mu\text{m}]-[4.6\mu\text{m}]=0.32$ mag and $[4.6\mu\text{m}]-[12\mu\text{m}]=4.24$ mag, are atypical for blazars or NLSy1 (cf. Fig. 2 from Paliya et al. 2018).

5.4. Nature of UGSC

Based on the whole set of data, the nature of the UGSC seems to be complex. The information on its polarization value may denote the existence of a relativistic jet attributed to an AGN. This hypothesis is supported by the shape of the SED and the possible emitting components that are typical for low-luminosity AGN. However, the near- to mid-infrared colors of UGSC are not consistent with this hypothesis and suggest a different type of source.

The UGSC lies below the Ka03 line in the BPT, but rather close to the composite objects' area. Based on the rest of the data presented above, we suggest that there is an AGN contribution to the UGSC emission. This argument is also supported by Kewley et al. (2006). As the authors discuss, an AGN contribution is likely on the condition that $\log(\frac{[\text{NII}]}{H_\alpha}) \geq -0.5$. Furthermore, based on Fig. 2 in the same work, the UGSC is consistent with the positions of an AGN on the $[\text{SII}]/H_\alpha$ diagram.

By inspection of the shape of the spectrum, UGSC could be categorized as a type 2 AGN. It is typical for this kind of active galaxy to display only narrow lines and a high degree of polarization, as observed, due to scattering from a dusty torus that obscures the nucleus (see, e.g., Tadhunter 2008). However, these objects usually have a ratio of $\log(\frac{[\text{OIII}]}{H_\beta}) \geq 0.48$ (Shuder & Osterbrock 1981).

The upper limit on the X-ray luminosity of UGSC ($\sim 7.4 \times 10^{41}$ erg/s) is consistent with a classification as a star-forming galaxy, but it cannot rule-out the possibility that it hosts a low-luminosity or a heavily obscured AGN. Finally, the optical light curve of the UGSC (Fig. 9) suggests that it can be a variable source, which strengthens the AGN argument. We conclude that the UGSC is most likely a composite object, i.e., a starburst galaxy with an AGN core.

6. Association with the *Fermi* field and other candidates

The UGSC could be the potential counterpart for the γ -ray field 3FGL J0221.2+2518, but a confident association is challenging. There are three other candidates proposed for this field. Schinzel et al. (2017) introduced two different counterparts. One of them is a known Radio Galaxy, NVSS J022126+251436, 2.3 arcmin away from UGSC, with AGN-like spectral energy distribution and variable optical flux (labeled 'RG' in Fig. 5). This source is listed in SDSS DR8 as a $r = 19.05$ mag source and its polarization degree is consistent with zero due to high measurements uncertainties. In Fig. 9 we show the Palomar Transient Factory r-band light curve of this source together with the light curve of the UGSC.

³ <http://heasarc.gsfc.nasa.gov/ftools/>

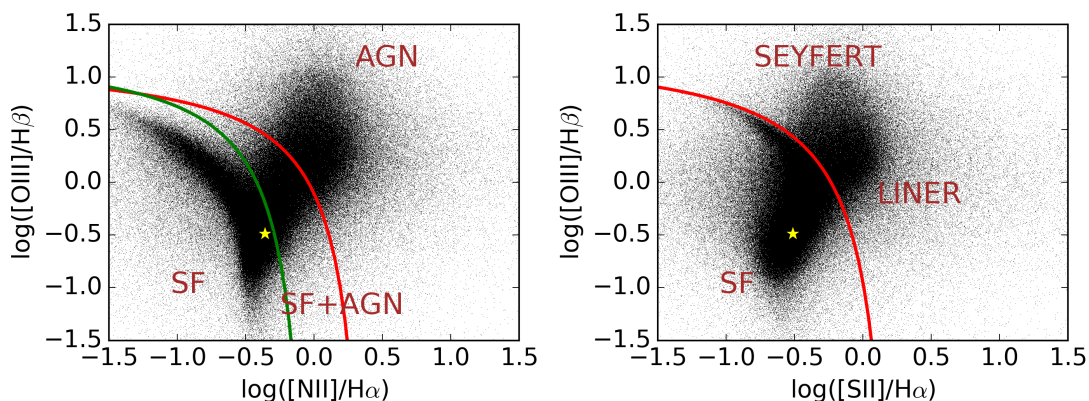


Fig. 7. Baldwin-Phillips-Terlevich diagrams according to the Kewley et al. (2006) classification scheme, produced using SDSS DR7 data. The yellow star indicates the position of UGSC in the diagrams. The error bars are smaller than the symbol size and thus cannot be depicted. The red curve (Ke01) denotes the demarcation between star-forming galaxies and AGN as defined by Kewley et al. (2001). The green curve (Ka03) shows the same demarcation as defined by Kauffmann et al. (2003). SF stands for a star-forming galaxy region.

The second counterpart by Schinzel et al. (2017) is proposed to be a radio source located at RA=02h21m15.67s, Dec=+25°16′58.48″. Its position is labeled ‘X’ in Fig. 5 and is denoted as a radio source. There is no known source within the 0.3″ error radius they propose in optical catalogs or in our dataset. The source can be fairly faint and only detectable in radio band. Given the lack of information regarding this source, we cannot exclude the possibility that it is associated with the 3FGL J0221.2+2518 field.

Finally, we examined the work by Massaro et al. (2016), who report that they have identified a counterpart for 3FGL J0221.2+2518. They collected optical spectroscopic data for the counterpart proposed by Paggi et al. (2014) for this field, and classified it as a QSO. The QSO is located at RA=02h20m51.24s, Dec=+25°09′27.6″, which places it at $\sim 5\sigma$ uncertainty ellipse of the *Fermi* field. It is not shown in Fig. 5 since it is relatively far from the center of the γ -ray field. Given the location of the QSO with respect to the UGS position and its uncertainties, it is extremely unlikely ($\varphi = 6 \times 10^{-7}$) that this AGN can be associated with the UGS.

7. Conclusions

We proposed optical polarimetry as a fast and efficient tool for identifying blazars in a high-polarization state as possible counterparts of γ -ray sources from the *Fermi*-LAT catalogue. This technique can serve as a powerful addition to a variety of previously proposed methods. Moreover, it can be improved by using multiple measurements of a given field at different epochs. Thus, variability of polarization (another distinct property of blazars) can be used for their identification.

We measured the optical polarization of sources in the 3FGL J0221.2+2518 field and discovered a new extragalactic source positioned at RA=02h21m33.3s, Dec=+25°12′47.3″, with redshift $z=0.0609 \pm 0.0004$. Its fractional polarization $5.2 \pm 1.3\%$ is significantly higher than the average polarization of the field $0.91 \pm 0.07\%$. Analysis of the multiband archival data in combination with optical spectroscopy leads us to the conclusion that the source is most likely a complex source comprised of an AGN along with a star-forming region in its galaxy.

This result confirms our theoretical estimates, demonstrates the usefulness of our method, and motivates its use for future research. The upcoming large polarimetric survey *PASIPHAЕ* (Tassis et al. 2018) aims to map the polarization of millions

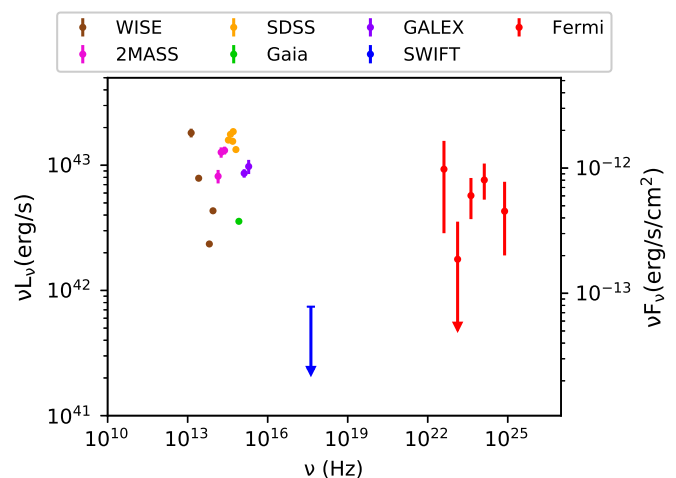


Fig. 8. Spectral energy distribution for the UGSC and γ -ray data for 3FGL J0221.2+2518 from 3FGL. Red points correspond to *Fermi* data for the UGS, while the others correspond to measurements for UGSC.

of objects in both the northern and the southern hemispheres. *PASIPHAЕ* will provide an exceptional opportunity to discover many previously unknown synchrotron emitters, including dozens of candidate counterparts for unidentified *Fermi*-LAT sources.

Acknowledgements. We thank Richard Britto and Marcello Giroletti for useful comments that improved this work. We thank the Swift Observatory Team, in particular Brad Cenko, for their rapid approval and scheduling of ToO observations. The *RoboPol* project is a collaboration between Caltech in the USA, MPIfR in Germany, Toruń Centre for Astronomy in Poland, the University of Crete/FORTH in Greece, and IUCAA in India. D.B. acknowledges support from the European Research Council (ERC) under the European Union’s Horizon 2020 research and innovation program under grant agreement No 771282. G. V.P. acknowledges support by the European Commission Seventh Framework Programme (FP7) through the Marie Curie Career Integration Grant PCIG-GA-2011-293531 “SFOnset”. K.K., A.Z., and R.S. acknowledge funding from the European Research Council under the European Union’s Seventh Framework Programme (FP/2007-2013)/ERC Grant Agreement n. 617001. This research has made use of the NASA/IPAC Infrared Science Archive, which is operated by the Jet Propulsion Laboratory, California Institute of Technology, under contract with the National Aeronautics and Space Administration. This publication makes use of data products from the Wide-field Infrared Survey Explorer, which is a joint project of the University of California, Los Angeles, and the Jet Propulsion Laboratory/California Institute of Technology, funded by the National Aeronautics and

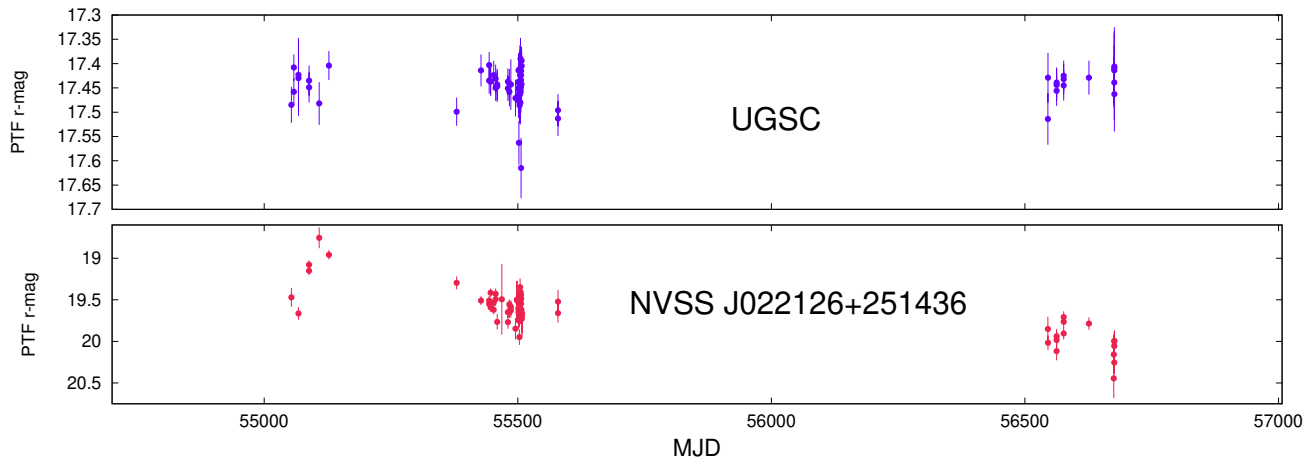


Fig. 9. Optical light curves of UGSC and NVSS J022126+251436 from the Palomar Transient Factory.

Space Administration This research has made use of the SVO Filter Profile Service (<http://svo2.cab.inta-csic.es/theory/fps/>) supported by the Spanish MINECO through grant AyA2014-55216, The SVO Filter Profile Service (Rodrigo, C., Solano, E., Bayo, A. <http://ivoa.net/documents/Notes/SVOFPS/index.html>) and The Filter Profile Service Access Protocol (Rodrigo, C., Solano, E. <http://ivoa.net/documents/Notes/SVOFPSDAL/oke-index.html>).

References

- Acero, F., Donato, D., Ojha, R., et al. 2013, *ApJ*, 779, 133
 Acero, F. et al. 2015, *ApJS*, 218, 23
 Andersson, B.-G., Lazarian, A., & Vaillancourt, J. E. 2015, *ARA&A*, 53, 501
 Angel, J. R. P. & Stockman, H. S. 1980, *ARA&A*, 18, 321
 Angelakis, E., Hovatta, T., Blinov, D., et al. 2016, *MNRAS*, 463, 3365
 Baldwin, J. A., Phillips, M. M., & Terlevich, R. 1981, *PASP*, 93, 5
 Barr, E. D., Guillemot, L., Champion, D. J., et al. 2013, *MNRAS*, 429, 1633
 Blackburn, J. K. 1995, in *Astronomical Society of the Pacific Conference Series*, Vol. 77, *Astronomical Data Analysis Software and Systems IV*, ed. R. A. Shaw, H. E. Payne, & J. J. E. Hayes, 367
 Blandford, R. D. & Königl, A. 1979, *ApJ*, 232, 34
 Blinov, D., Pavlidou, V., Papadakis, I. E., et al. 2016, *MNRAS*, 457, 2252
 Burrows, D. N., Hill, J. E., Nousek, J. A., et al. 2005, *Space Sci. Rev.*, 120, 165
 Chiaro, G., Salvetti, D., La Mura, G., et al. 2016, *MNRAS*, 462, 3180
 Cohen, D. P., Romani, R. W., Filippenko, A. V., et al. 2014, *ApJ*, 797, 137
 Dickey, J. M. & Lockman, F. J. 1990, *ARA&A*, 28, 215
 Doert, M. & Errando, M. 2014, *ApJ*, 782, 41
 Foschini, L., Angelakis, E., Fuhrmann, L., Ghisellini, G., et al. 2012, *A&A*, 548, A106
 Frail, D. A., Mooley, K. P., Jagannathan, P., & Intema, H. T. 2016, *MNRAS*, 461, 1062
 Halonen, R. J., Mackay, F. E., & Jones, C. E. 2013, *ApJS*, 204, 11
 Heiles, C. 2000, *AJ*, 119, 923
 Hiltner, W. A. 1956, *ApJS*, 2, 389
 Kauffmann, G., Heckman, T. M., Tremonti, C., et al. 2003, *MNRAS*, 346, 1055
 Kewley, L. J., Dopita, M. A., Sutherland, R. S., Heisler, C. A., & Trevena, J. 2001, *ApJ*, 556, 121
 Kewley, L. J., Groves, B., Kauffmann, G., & Heckman, T. 2006, *MNRAS*, 372, 961
 King, O. G. et al. 2014, *MNRAS*, 442, 1706
 Kovalev, Y. Y. 2009, *ApJ*, 707, L56
 Liidakis, I., Romani, R. W., Filippenko, A. V., et al. 2018, *MNRAS*, 480, 5517
 Massaro, F., Alvarez Crespo, N., D’Abrusco, R., et al. 2016, *Ap&SS*, 361, 337
 Oudmaijer, R. D., Palacios, J., Eiroa, C., et al. 2001, *A&A*, 379, 564
 Paggi, A., Milisavljevic, D., Masetti, N., et al. 2014, *AJ*, 147, 112
 Paliya, V. S., Ajello, M., Rakshit, S., et al. 2018, *ApJ*, 853, L2
 Panopoulou, G., Tassis, K., Blinov, D., et al. 2015, *MNRAS*, 452, 715
 Park, T., Kashyap, V. L., Siemiginowska, A., et al. 2006, *ApJ*, 652, 610
 Pavlidou, V. et al. 2014, *MNRAS*, 442, 1693
 Planck Collaboration, Ade, P. A. R., Aghanim, N., et al. 2016, *A&A*, 594, A13
 Salvetti, D., Chiaro, G., La Mura, G., & Thompson, D. J. 2017, *MNRAS*, 470, 1291
 Schinzel, F. K., Petrov, L., Taylor, G. B., & Edwards, P. G. 2017, *ApJ*, 838, 139
 Schlafly, E. F. & Finkbeiner, D. P. 2011, *ApJ*, 737, 103
 Schlafly, E. F., Green, G., Finkbeiner, D. P., et al. 2014, *ApJ*, 789, 15
 Schlegel, D. J., Finkbeiner, D. P., & Davis, M. 1998, *ApJ*, 500, 525
 Shuder, J. M. & Osterbrock, D. E. 1981, *ApJ*, 250, 55
 Sowards-Emmerd, D., Romani, R. W., & Michelson, P. F. 2003, *ApJ*, 590, 109
 Tadhunter, C. 2008, *New A Rev.*, 52, 227
 Tassis, K., Ramaprakash, A. N., Readhead, A. C. S., et al. 2018, *ArXiv e-prints* [[arXiv:1810.05652](https://arxiv.org/abs/1810.05652)]